

Watch Closely: Mitigating Object Hallucinations in Large Vision-Language Models with Disentangled Decoding

Ruiqi Ma¹, Yu Yan¹, Chunhong Zhang¹, Minghao Yin²,
XinChao Liu¹, Zhihong Jin¹, Zheng Hu¹

¹Beijing University of Posts and Telecommunications

²The University of Hong Kong

Abstract

Large Vision-Language Models (LVLMs) bridge the gap between visual and linguistic modalities, demonstrating strong potential across a variety of domains. However, despite significant progress, LVLMs still suffer from severe hallucination issues in object recognition tasks. These models often fail to accurately identify certain objects, leading to text generation that appears fluent but does not correspond to the visual content, which can have serious consequences in real-world applications. Recently, several methods have been proposed to alleviate LVLM hallucinations, but most focus solely on reducing hallucinations in the language modality. To mitigate hallucinations in both the language and visual modalities, we introduce Hallucination Disentangled Decoding (HDD) method that requires no training. HDD enhances the original image by segmenting it and selecting images that augment the original, while also utilizing a blank image to eliminate language prior hallucinations in both the original and segmented images. This design not only reduces the model's dependence on language priors but also enhances its visual performance. (Code: <https://github.com/rickeyhhh/Hallucination-Disentangled-Decoding>)

1 Introduction

Large Vision-Language Models (LVLMs) (Yin et al., 2023) typically consist of a large language model and a visual encoder or multimodal vision model. The visual module effectively captures feature information from images and maps this visual information to text in a shared space (Dosovitskiy et al., 2020). Leveraging their remarkable image processing capabilities, LVLMs have already demonstrated significant value across various domains. However, challenges remain, with one of the most prominent being the issue of multimodal hallucination. The multimodal hallucination prob-

lem in LVLMs is primarily manifested in the inability of the text output to accurately correspond to the input image information, including the generation of non-existent objects and errors in object recognition. This issue undermines the model's reliability to some extent.

Some studies have already investigated "how hallucinations arise," revealing the LVLM's potential over-reliance on the language priors of the backbone language model (Yue et al., 2024) and biases in the training datasets (Liu et al., 2024a). Recently, many approaches have been proposed to alleviate such multimodal hallucinations, including manually constructing negative samples for contrastive decoding (Leng et al., 2023), identifying summary tokens generated during LVLM output and applying penalty mechanisms (Huang et al., 2023), as well as training methods that encourage the generation of EOS tokens to prevent the model from producing overly detailed or hallucinated content (Yue et al., 2024). While these methods have alleviated LVLM hallucinations to some extent, multimodal hallucination remains an entangled phenomenon, originating from both of the LVLM's main components: the visual and language modules, each of which generates its own type of hallucination. The visual module has limitations in its perceptual capabilities and may fail to accurately recognize smaller objects in highly informative images (Kan et al., 2024). The language module, due to its autoregressive nature, tends to emphasize linguistic coherence (Liu et al., 2024b) when generating the next token, rather than ensuring correspondence between the text and the image. The aforementioned methods have not disentangled the sources of LVLM hallucinations, but rather address hallucinations in a coarse-grained manner, which can lead to a performance trade-off when alleviating hallucinations in one module at the cost of another. To address this issue, we propose a approach by disentangling the analysis of the sources of hallucinations in the

LVLM’s visual and language modules.

In this work, we designed experiments to analyze the sensitivity of LVLMs to local image details, leading to the conclusion that the sensitivity of the LVLM’s visual encoder to entities in the image is correlated with the size of the entities (Zhang et al., 2024). During the course of these experiments, we also identified and analyzed the LVLM’s dependency on language priors, which aligns with previous research findings (Wang et al., 2024). Through this research, we decompose the entangled concept of LVLM hallucinations into two clearer components: visual hallucinations (Guan et al., 2023) and language hallucinations (Liu et al., 2024a). To address these two sources of hallucinations, we propose a disentangled decoding approach to reduce LVLM hallucinations. We segment the original image and enhance the original image by calculating the Jensen-Shannon divergence (Fuglede and Topsøe, 2004) between the segmented image and the original image, as well as contrastive decoding (Wang et al., 2024) using blank images to eliminate the LVLM’s reliance on language priors. Our approach is highly effective, outperforming recent methods and baselines across multiple hallucination benchmark tests.

Overall, our contributions are as follows:

1. We conducted an in-depth study of the LVLM’s sensitivity to local image details and analyzed its excessive reliance on language priors.
2. We propose the Hallucination Disentangled Decoding method, which overcomes the limitations of previous approaches that were unable to disentangle and eliminate hallucinations from both visual and language modules.
3. Through various benchmark tests, HDD demonstrates superior perceptual capabilities and generates fewer hallucinations without any additional training or fine-tuning.

2 Related Work

2.1 Hallucinations in LVLMs

Multimodal hallucinations include object hallucinations, attribute hallucinations, relation hallucinations (Bai et al., 2024), etc. Here we mainly focus on object hallucinations. There are two main causes of LVLM’s object hallucinations, (1) Limited perceptual capabilities of the visual module

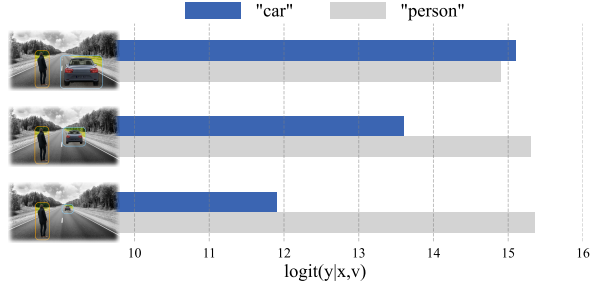


Figure 1: The figure above illustrates the impact of different object sizes in the image on the model’s output logits distribution. From top to bottom, the area of the “car” gradually decreases, while the area of the “person” remains unchanged, serving as a control.

(Liu et al., 2024a). For entities occupying a small area in the image, the visual module may struggle to perceive them in detail, leading to either omission or incorrect descriptions. Of course, there are many factors that influence the limitations of the visual module, such as training data contamination (Yu et al., 2023), overly detailed annotations (Yue et al., 2024), and data biases (Liu et al., 2024a). (2) Excessive reliance of the language module on the language priors of the backbone LLM (Chen et al., 2025). The proportion of image information decreases during the sequence generation process (Yue et al., 2024), which is a characteristic of autoregressive models. Hallucinations generated by the visual encoder can induce the language model to generate more hallucinations, causing these two types of hallucinations to often be entangled.

2.2 Hallucination Mitigation Methods

Recently, numerous efforts have focused on mitigating object hallucinations in LVLMs through the design of different decoding strategies. OPERA (Huang et al., 2023) introduces a decoding approach that adjusts attention weights with a penalty term and incorporates a fallback mechanism to suppress the influence of aggregate tokens during generation. VCD (Leng et al., 2023) introduces visual noise to construct negative samples and employs contrastive decoding to reduce hallucinations. HALC (Chen et al., 2024) leverages an auxiliary vision model to identify hallucinated tokens and performs multi-scale resampling over the input image to refine the output distribution. SID (Huo et al., 2025) mitigates hallucinations via token-level perturbation-induced decoding, while RITUAL (Woo et al., 2024) employs randomized image transformations to suppress hallucinated

content. In this work, we propose the first disentangled framework for hallucination mitigation in LVLMs. Our approach leverages semantic segmentation model to construct additional structured visual input and employs blank images to eliminate the model’s reliance on language priors, effectively mitigating the hallucinations between visual and language modules. The proposed method is intuitive, highly interpretable, and achieves state-of-the-art performance across various evaluation metrics.

3 Preliminary

3.1 Decoding in LVLMs

We model the LVLM as a function \mathcal{M}_θ , where the input consists of an image input v and a text query input x . Mathematically, at the t -th decoding step, the auto-regressive process can be represented as:

$$y_t = \mathcal{M}_\theta(v, x, y_{<t}) \quad (1)$$

$y_{<t}$ represents the results decoded in the previous $t-1$ steps, where the next token is predicted based on the previously generated tokens. We can expand Equation 1 as follows:

$$p(y_t|v, x, y_{<t}) = \text{SoftMax}[\text{logit}(y_t|v, x, y_{<t})] \quad (2)$$

$$y_t \sim p(y_t|v, x, y_{<t}) \quad (3)$$

For simplicity of representation, the processing of the visual encoder and the text encoder is not shown here. The model generates the logits distribution for the next token based on the image information v , the query x , and the previously generated tokens $y_{<t}$. This logit distribution is then normalized into a probability distribution via SoftMax, and a token is selected using specific sampling strategy. Hallucinations can arise at two stages, (1) the local detail bias in the output v after the image input passes through the visual encoder, and (2) the language prior bias introduced by the iteratively generated preceding tokens $y_{<t}$. Our method addresses these two challenges separately.

3.2 Semantic Segmentation Tool

We construct additional visual information by leveraging semantic segmentation tools to automatically generate entity-level masks and partition the input image accordingly. In our main experiments, we adopt the Segment Anything Model (Kirillov et al., 2023) as the primary segmentation backbone. For ablation studies, we further compare the effectiveness of our framework when integrated with alternative segmentation models, including Mask2Former (Cheng et al., 2022) and Mask R-CNN (He et al.,

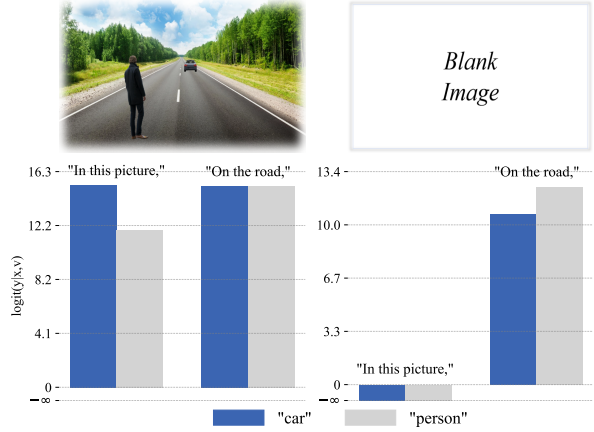


Figure 2: The figure above demonstrates the impact of different prompt inputs on the model’s output. It explains the phenomenon of "Decoding Inertia" by introducing a blank image and two distinct prompt inputs.

2018). The partitioning process can be expressed as:

$$\text{Seg}(v) = \sum_{i=1}^n (\text{Mask}_i \odot v) \quad (4)$$

where v represents the image input to the segmentation model. After processing, the image v produces n masks, which are multiplied pixel-wise with the original image. Each result represents a distinct entity, and by combining these entities, a new additional visual image is obtained.

3.3 Local Detail-Induced Hallucinations

The precision of the visual input is crucial to determine whether an LVLM generates hallucinations. However, the visual encoder exhibits lower sensitivity to entities that occupy a small area in the image (Liu et al., 2021), often misrepresenting or failing to capture these small entities, leading to the generation of hallucinations. For LVLM, this phenomenon is also documented in (Zhang et al., 2024), where the uniform image resolution input setting of the visual encoder leads to the models lacking the same sensitivity to scale and detail as human vision. In the following, we will delve into the LVLM’s sensitivity to entities with different area proportions in the image, and we will provide experimental evidence to support the validity of this hypothesis.

Insensitivity to Local Details. To demonstrate the model’s sensitivity to local details, we designed an experiment in which three images of a "car" were created at varying distances, meaning the "car" progressively becomes smaller. A "person" of constant size was used as a comparison. Figure 1 presents

the three images, and we extracted the logits corresponding to the same query from the LVLM’s feedback. The volume of the “*person*” entity remains unchanged across all three images, and the corresponding logits show minimal variation. However, the logits for the “*car*” entity almost linearly change in proportion to its size. This observation indicates a correlation between the LVLM’s visual encoder sensitivity and the size of the entities in the image: $\text{logit}_i \propto \frac{A_i}{A_{\text{all}}}$, (A represents the area of the region.) As shown in Equation 2, visual information biases influence the model’s reasoning process, which in turn exacerbates hallucinations caused by language priors.

“Decoding Inertia”: LVLM’s Over-reliance on Language Priors. Interestingly, during the above experiment, we found that replacing the opening phrase “*In this picture*,” with “*On the road*,” in the prompt led to a significant shift in the LVLM’s output distribution. As shown in Figure 2, when we altered the prompt and tested the image with the smallest “*car*” entity, the logit for the “*car*” output significantly increased. To further investigate this phenomenon, we conducted an experiment with a blank image, using both prompt settings to query the LVLM. The logit results confirmed our hypothesis that the LVLM over-relies on language priors. When the word “*road*” appeared, the probability of the “*car*” entity also increased substantially. We refer to this phenomenon as “Decoding Inertia”, which may be due to the frequent co-occurrence of specific objects in training data (Zhou et al., 2024; Galleguillos et al., 2008).

4 Method

4.1 Hallucination Disentangled Decoding

From the experiments in the previous section, we found that both the vision module and the language module had shortcomings that could not be ignored, and the previous work was optimized for only one module. To address this issue, we propose Hallucination Disentangled Decoding (HDD), which aims to decouple and mitigate hallucinations in both the visual and language modules of the LVLM.

4.1.1 Visual Detail Enhancement

For hallucinations in the visual module, in order to amplify the proportion of local details in the image information, we use semantic segmentation model to segment the original image into two complemen-

tary images:

$$v_1 = \sum_{i=1}^N (\text{Mask}_i \odot \mathcal{V}), v_2 = \mathcal{V} - v_1 \quad (5)$$

\mathcal{V} represent the original image, and v_1 and v_2 represent the two complementary segmented images. This approach effectively increases the proportion of the queried entity in the original image. The image segmentation strategy is selecting the largest N masks as the first image (if there is no special statement: $N = 0.05 * n$), and then masking the entities in the first image from the original, with the remaining entities forming the second image. Additionally, a completely blank image v_n is introduced. These four images: v , v_1 , v_2 , and v_n are then used as inputs to the LVLM, generating four different output distributions. Our goal is to automatically select the most effective segmented image to answer the query. To achieve this, we use the Jensen-Shannon divergence (Fuglede and Topsøe, 2004) to measure the differences between v_1 , v_2 and v_n .

$$\text{Div}_i = \text{JSD} \left[p(y_t|v_i, x, y_{<t}) \parallel p(y_t|v_n, x, y_{<t}) \right] \quad (6)$$

where $i \in (1, 2)$. A larger Div indicates a greater difference between the segmented image and the blank image, meaning that this segmented image contains more effective information. We use the segmented image with the larger Div to enhance the original image by adding the logit distribution of the selected segmented image to the logit distribution of the original image.

Adaptive Weight Soft Adjustment We also design an automatic weight adjustment mechanism to adaptively control the extent of local detail enhancement. From a mathematical perspective, we have:

$$\delta = |\text{Div}_1 - \text{Div}_2| \quad (7)$$

δ allows the segmented image containing more effective information to provide stronger guidance to the original image, while conversely, the segmented image with less effective information exerts a weaker influence on the original image. Combining this with the previously discussed local detail enhancement, we have enhanced logit:

$$\text{logit}_{\text{enh}}(\mathcal{V}) = (1 - \delta) \cdot \text{logit}(\mathcal{V}) + \delta \cdot \text{logit}(v_{i^*}), \quad (8)$$

where $i^* = \arg \max \text{Div}_i, i \in \{1, 2\}$

4.1.2 Language Prior Elimination

In the previous section, we enhanced the capability of the LVLM’s visual module. However, as demonstrated in the experiment shown in Figure 2, both the original image and the segmented image in the

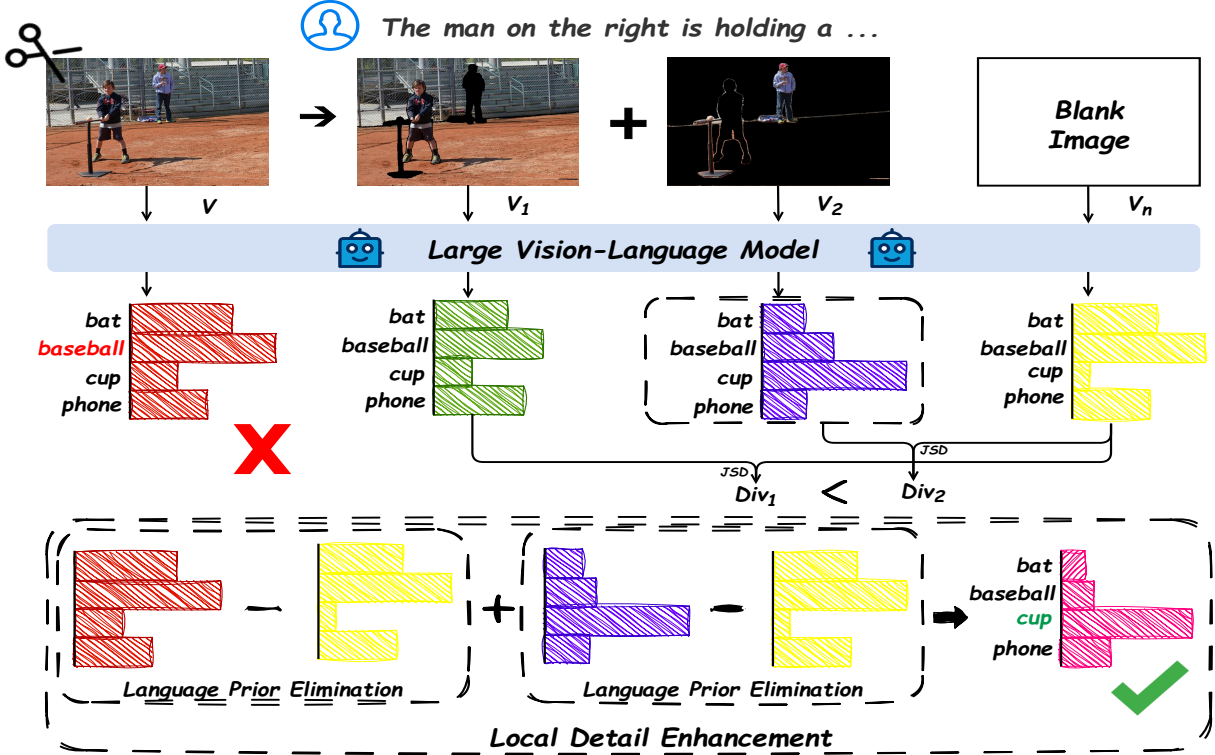


Figure 3: This figure provides an overview of Hallucination Disentangled Decoding. First, the original image is segmented into two images. The blank image, along with the three aforementioned images, is then input into the LVLM, and their respective output distributions are obtained. By calculating the Jensen-Shannon (JS) divergence between the distributions of the two images and the blank image, the image with the higher JS divergence is selected. The original image and the chosen image are then subtracted from the blank image’s distribution and summed to obtain the new output distribution.

LVLM can exhibit an over-reliance on language priors. To solve this problem, we introduce a blank image, serving as an image placeholder. This operation allows the LVLM to degrade into a simple language-only model, where the query input can elicit hallucinations based solely on language priors (since there is no visual input). Based on the analysis above, we perform contrastive decoding (Wang et al., 2024) by subtracting the output distribution of the blank image v_n from the output distribution of the image input, and add a weighting factor α . Mathematically, this can be formulated as:

$$\text{logit}^*(v_{in}) = (1+\alpha) \cdot \text{logit}_{enh}(v_{in}) - \alpha \cdot \text{logit}_{enh}(v_n) \quad (9)$$

Here, v_{in} includes the original image \mathcal{V} as well as the segmented images v_1 and v_2 . Combining the local detail enhancement from the previous section, we finally have logits:

$$\text{logit}_{hdd} = (1 - \delta) \cdot \text{logit}^*(\mathcal{V}) + \delta \cdot \text{logit}^*(v_{i^*}), \quad (10)$$

where $i^* = \arg \max \mathcal{D}_{Div_i}, i \in \{1, 2\}$

Our final logits as shown in Figure 3 incorporate both the enhancement of the visual module and the elimination of language priors, effectively disentangling and mitigating hallucinations in both

modules. This approach avoids compromising the performance of any module when reducing hallucinations, as well as other potential adverse effects.

5 Experiments

In this section, we evaluate the effectiveness of Hallucination Disentangled Decoding using multiple LVLMs and various benchmark tests.

5.1 Experimental Settings

Evaluation Metrics

POPE Polling-based Object Detection Evaluation (Li et al., 2023) is a recently introduced method aimed at assessing hallucination issues in LVLMs. POPE focuses on evaluating object hallucinations by converting the hallucination assessment metric into a binary classification task using a question like *"Is there a <object> in the image?"* to determine whether the model can correctly identify an object corresponding to a given image. The POPE test consists of three parts: The "random" setting randomly selects objects from the entire dataset for querying. The "popular" setting queries the

Dataset	Spilt	Method	LLaVA-1.5		InstructBLIP		LLaVA-NeXT	
			Acc. \uparrow	F1 \uparrow	Acc. \uparrow	F1 \uparrow	Acc. \uparrow	F1 \uparrow
MS COCO	Random	Greedy	88.7	87.3	87.0	86.3	89.3	88.8
		+VCD	88.7	88.3	86.5	85.9	87.8	87.0
		+SID	89.5	89.6	87.2	87.0	90.0	90.0
		+HDD	90.1	90.0	89.2	88.7	91.5	91.3
	Popular	Greedy	82.7	83.3	84.7	84.2	84.1	81.7
		+VCD	87.3	87.1	84.3	83.8	87.7	87.6
		+SID	87.1	87.2	85.1	85.4	88.2	87.5
		+HDD	88.0	88.0	87.0	86.8	89.2	89.0
A-OKVQA	Adversarial	Greedy	81.1	80.7	80.0	80.1	83.2	81.0
		+VCD	81.4	82.2	80.1	80.5	82.9	81.5
		+SID	82.7	81.9	81.4	80.9	84.0	83.0
		+HDD	83.3	83.4	82.3	82.5	84.3	84.5
	Random	Beam	86.3	87.4	88.3	88.4	86.6	85.3
		+VCD	87.2	88.2	87.6	87.7	87.4	88.0
		+OPERA	85.7	86.9	89.0	89.4	86.3	87.2
		+HALC	88.2	87.4	88.4	87.7	89.0	88.2
GQA	Popular	+HDD	89.5	89.4	88.4	88.5	89.5	89.6
		Beam	78.7	81.7	81.0	82.2	84.5	83.3
		+VCD	79.5	82.6	80.8	81.9	84.8	86.7
		+OPERA	79.9	82.5	79.5	81.8	84.3	85.0
	Adversarial	+HALC	84.7	84.3	81.4	80.8	85.9	84.7
		+HDD	85.0	85.1	81.6	82.9	86.8	87.2
		Beam	68.1	74.9	74.7	77.9	78.6	78.3
		+VCD	75.8	78.6	74.9	77.6	78.7	78.9
GQA	Random	+OPERA	69.1	75.4	71.5	76.4	78.4	79.1
		+HALC	77.5	79.6	74.9	77.2	78.7	79.2
		+HDD	78.0	79.9	75.7	79.0	79.1	79.5
		Sampling	83.5	82.7	79.5	80.4	83.1	81.2
	Popular	+VCD	86.1	87.1	82.8	83.2	85.7	85.9
		+RITUAL	86.8	87.2	83.5	84.3	88.7	88.9
		+HDD	87.2	87.6	84.1	84.9	89.3	89.4
		Sampling	78.1	78.3	73.5	76.1	78.2	77.1
GQA	Adversarial	+VCD	80.1	81.6	76.8	78.6	80.3	81.1
		+RITUAL	79.5	79.8	76.7	78.7	84.4	86.2
		+HDD	80.5	81.3	77.0	80.1	86.8	87.3
		Sampling	74.8	75.8	70.4	74.1	75.4	74.7
	Adversarial	+VCD	75.2	77.7	73.1	76.1	75.8	76.5
		+RITUAL	75.3	76.1	72.8	75.5	77.2	78.3
		+HDD	76.4	78.1	73.5	76.0	78.4	80.5

Table 1: The results of the POPE evaluation. We tested three different decoding strategies across various baselines and HDD. The best results are highlighted in bold.

most frequently occurring objects in the evaluation dataset. The "adversarial" setting queries objects that are highly relevant to the entities appearing in the image.

CHAIR Caption Hallucination Assessment with Image Relevance (Rohrbach et al., 2018) is used to evaluate the accuracy of model outputs. This framework includes two evaluation dimensions: the sentence dimension (CHAIR_S) and the entity dimension (CHAIR_I). CHAIR_S represents the sentence-level evaluation, measuring the proportion of hallucinated sentences relative to all generated sentences, while CHAIR_I measures the object-

instance level hallucination, indicating the proportion of hallucinated objects relative to all generated objects. For different settings, we used the same prompt: *"Please describe this image in detail."*

GPT-4 Assisted Benchmark POPE and CHAIR are both effective objective metrics, but they primarily focus on the object-existence-level hallucination and are unable to effectively capture hallucinated information related to entity relationships and spatial positions. Therefore, we introduce the GPT-4 Assisted Benchmark (Zhao et al., 2023), which leverages LVLM-generated detailed descriptions of the VG dataset to measure hallucinations

Method	LLaVA-1.5			InstructBLIP			LLaVA-NeXT		
	CHAIR _I ↓	CHAIR _S ↓	Length	CHAIR _I ↓	CHAIR _S ↓	Length	CHAIR _I ↓	CHAIR _S ↓	Length
Multinomial Sampling	7.9	26.4	53.4	10.4	32.8	53.9	7.5	18.0	60.1
Greedy Decoding	6.0	21.0	54.7	7.3	26.2	55.4	6.0	14.8	60.7
Beam Search	5.9	20.8	54.5	7.1	25.8	55.3	5.7	14.4	60.4
VCD	6.4	22.4	54.3	6.3	24.0	54.4	6.1	15.1	60.2
OPERA	6.1	21.4	54.1	7.3	22.4	52.7	5.7	14.7	59.8
HALC	6.2	22.0	54.5	6.8	23.2	54.7	5.8	14.9	60.3
HDD	5.6	18.4	52.7	6.3	21.2	55.5	5.5	13.6	60.2

Table 2: The results of the CHAIR evaluation are presented. We tested various baselines and HDD on two different models, with all tests conducted under the condition of *max new tokens* = 64.

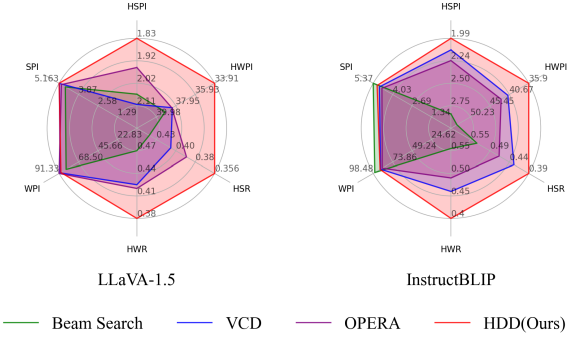


Figure 4: GPT-4 assisted hallucination evaluation results on VG dataset. We analyse the results across six dimensions, where HWR, HSR, HSPI, and HWPI are better when lower, while WPI and SPI are better when higher. Overall, a larger proportion on the radar chart indicates better performance.

in a more fine-grained manner. The benchmark using GPT-4 (Achiam et al., 2023) and includes six evaluation dimensions: the number of sentences per image (SPI), the number of words per image (WPI), the number of hallucinated sentences per image (HSPI), the number of hallucinated words per image (HWPI), the ratio of hallucinated sentences (HSR) and the ratio of hallucinated words (HWR). More details are in Appendix A.

Models and Datasets

Based on prior work, we selected LLaVA-v1.5-7b (Liu et al., 2023), InstructBLIP-7b (Dai et al., 2023) and LLaVA-NeXT (Li et al., 2024). Our evaluation metrics involve four different datasets: MS-COCO (Lin et al., 2014), A-OKVQA (Schwenk et al., 2022), GQA (Hudson and Manning, 2019) and Visual Genome (VG) dataset (Krishna et al., 2016).

Baselines

We compare HDD with several advanced decoding methods, including: VCD (Wang et al., 2024), OPERA (Huang et al., 2023), HALC (Chen et al., 2024), SID (Huo et al., 2025) and RITUAL (Woo

et al., 2024). For all baselines, we performed a fair comparison using the hyperparameters recommended by each work.

5.2 Experimental Results

POPE Results Our method is fully adaptable to various decoding strategies. The results of all POPE evaluations are presented in Table 1. It is evident that HDD consistently outperforms all baseline methods across almost all LVLMs, datasets, and decoding strategies (up to +9.9 Acc., +10.2 F1). In some cases, VCD and OPERA even show lower recognition accuracy than vanilla models, which is consistent with the results in (Huo et al., 2025). This suggests that our method not only eliminates hallucinations caused by language priors but also enhances the object recognition capabilities of LVLMs.

CHAIR Results For the CHAIR evaluation, we randomly selected 500 images from the MSCOCO dataset as the query set. As shown in the results from Table 2, our method achieves more accurate and detailed expression in real image recognition tasks, with both CHAIR_I and CHAIR_S outperforming all baseline results. Notably, our method significantly reduces CHAIR_I and CHAIR_S (with a maximum improvement of 29.1% and 30.3% respectively), indicating that HDD can more accurately recognize entities in the image and make more precise judgments for ambiguous entities.

GPT-4 Benchmark Results From the Figure 4, we can observe that HDD significantly outperforms all baselines on the hallucination metrics. It surpasses VCD by 12.9% in the ratio of hallucinated sentences (HSR) and OPERA by 18.3% in the ratio of hallucinated words (HWR). This indicates that our approach breaks through the bottlenecks of previous methods that only address hallucinations in a single module. Furthermore, as observed WPI and SPI, HDD eliminates hallucinations without sacrificing the detail of image descriptions.



Greedy Decoding:

The image features a person wearing a green jacket, sitting on a ski lift handle holding a pair of skis. The skier is positioned in the middle of the scene, with the skis placed in front of them. The skis are attached to the person's feet, and they are likely preparing to ski down the slope. The ski lift is a prominent part of the scene, with the person sitting on a bench that is attached to the lift. The bench is located in the middle of the lift, providing a comfortable seating area for the skier.

Ours:

The image features a person wearing a green jacket, sitting on a ski lift with their skis attached. The skier is holding the ski lift handle, enjoying the ride up the mountain. The skis are placed on the person's feet, and the person appears to be looking down at the snow below. In the background, there is a snowboard visible, suggesting that the ski lift is also used by snowboarders. The scene captures the excitement and anticipation of skiing and snowboarding on the mountain.



Greedy Decoding:

The image features a small airplane parked on a dirt runway, with several people standing around it. There are at least nine people visible in the scene, some of them closer to the airplane while others are further away. A few of the people are carrying handbags, with three handbags visible in the scene. One handbag is located near the center of the image, another is closer to the left side, and the third one is near the right side. The group of people appears to be either preparing to board the airplane or has just disembarked from it.

Ours:

The image features a group of people gathered around a small airplane parked on a dirt field. There are at least nine people in the scene, with some standing closer to the airplane and others further away. They appear to be either preparing for a flight or just disembarking from the aircraft. The airplane is positioned in the center of the scene, with its nose pointing towards the left side. A golf cart is parked nearby, likely used for transportation or to carry luggage to and from the airplane. The overall atmosphere of the scene suggests a casual and friendly gathering of people around the small airplane.

Figure 5: The decoding differences on the MSCOCO dataset are presented, where the **Red** text highlights hallucinated regions, and the **Green** text represents additional detailed descriptions not present in the original decoding. Our method not only reduces hallucinated information but also provides more detailed descriptions.

Segmentation Tool	Random		Popular		Adversarial	
	Acc.↑	F1↑	Acc.↑	F1↑	Acc.↑	F1↑
SAM	90.1	90.0	88.0	88.0	83.3	83.4
Mask2Former	90.0	89.9	87.9	87.5	83.5	83.2
Mask R-CNN	89.8	89.9	87.5	87.4	83.0	83.1

Table 3: Ablation study of segmentation tools

5.3 Further Discussions

Impact of Segmentation Tools To demonstrate that our method is not dependent on a specific segmentation tool and is robust across different semantic segmentation models, we conduct an ablation study by replacing the primary segmentation backbone SAM with Mask2Former and Mask R-CNN. We perform POPE evaluation on the MSCOCO dataset using LLaVA-1.5 as shown in Table 3. Experimental results show that the choice of segmentation model has minimal impact on the final performance, with the largest accuracy difference being only 0.5%. This slight variation may stem from differences in segmentation granularity across models.

Computational Efficiency Comparison We measure the computational efficiency of different methods by the time each model requires to generate a single token. All experiments were conducted on a single NVIDIA RTX 4090 GPU. We sample inference times of LLaVA-1.5 on MSCOCO from the Chair evaluation and compute the corresponding output latencies. As shown in Figure 6, HDD operates within an acceptable efficiency range while demonstrating its effectiveness across various evaluations. HDD achieves latency comparable to VCD and base decoding methods, and significantly outperforms HALC and OPERA. These results indicate that HDD is a practical and efficient approach suitable for real-world scenarios.

Case Study on MSCOCO Figure 5 presents two

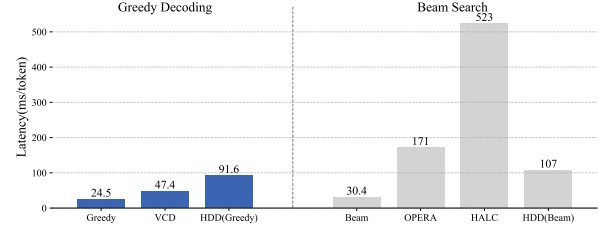


Figure 6: The decoding delay of different decoding methods, in ms/token. Higher values mean lower throughput.

samples of LLaVA-1.5 on MSCOCO. The red regions represent hallucinated information, while the green regions represent detailed information. Our method not only eliminates hallucinated information but also describes finer details in the image. HDD successfully identifies "ski lift handle" and "golf cart" and accurately analyzes the scene's intentions, such as "The skier is holding the ski lift handle, enjoying the ride up the mountain." and "A golf cart is parked nearby, likely used for transportation or to carry luggage to and from the airplane." These conclusions are drawn from observing the details of the scene.

6 Conclusion

In this paper, we propose a disentangled solution called Hallucination Disentangled Decoding (HDD). Through a fine-grained analysis of the sources of hallucinations in both visual and language modules of LLMs, we design two mechanisms to mitigate hallucinations in each module separately. (1) Using semantic segmentation model to segment images and enhance local details. (2) Using contrastive decoding with blank images to eliminate hallucinations caused by language priors. Our method outperforms existing methods in multiple benchmark tests and demonstrates superior robustness and generalizability.

7 Limitation

Although our approach achieves excellent results across various evaluations, there is still room for improvement. Our current research focuses on cross-modal alignment between images and text, without extending to other modalities such as video or 3D point clouds. While hallucinations remain prevalent in these modalities, we leave the exploration of applying our proposed method to mitigate hallucinations in broader multimodal settings as future work.

References

Josh Achiam, Steven Adler, Sandhini Agarwal, Lama Ahmad, Ilge Akkaya, Florencia Leoni Aleman, Diogo Almeida, Janko Altenschmidt, Sam Altman, Shyamal Anadkat, et al. 2023. Gpt-4 technical report. *arXiv preprint arXiv:2303.08774*.

Zechen Bai, Pichao Wang, Tianjun Xiao, Tong He, Zongbo Han, Zheng Zhang, and Mike Zheng Shou. 2024. Hallucination of multimodal large language models: A survey. *arXiv preprint arXiv:2404.18930*.

Cong Chen, Mingyu Liu, Chenchen Jing, Yizhou Zhou, Fengyun Rao, Hao Chen, Bo Zhang, and Chunhua Shen. 2025. Perturbollaava: Reducing multi-modal hallucinations with perturbative visual training. *Preprint*, arXiv:2503.06486.

Zhaorun Chen, Zhuokai Zhao, Hongyin Luo, Huaxiu Yao, Bo Li, and Jiawei Zhou. 2024. Halc: Object hallucination reduction via adaptive focal-contrast decoding. *Preprint*, arXiv:2403.00425.

Bowen Cheng, Ishan Misra, Alexander G. Schwing, Alexander Kirillov, and Rohit Girdhar. 2022. Masked-attention mask transformer for universal image segmentation. *Preprint*, arXiv:2112.01527.

Wenliang Dai, Junnan Li, Dongxu Li, Anthony Meng Huat Tiong, Junqi Zhao, Weisheng Wang, Boyang Albert Li, Pascale Fung, and Steven C. H. Hoi. 2023. Instructblip: Towards general-purpose vision-language models with instruction tuning. *ArXiv*, abs/2305.06500.

Alexey Dosovitskiy, Lucas Beyer, Alexander Kolesnikov, Dirk Weissenborn, Xiaohua Zhai, Thomas Unterthiner, Mostafa Dehghani, Matthias Minderer, Georg Heigold, Sylvain Gelly, Jakob Uszkoreit, and Neil Houlsby. 2020. An image is worth 16x16 words: Transformers for image recognition at scale. *ArXiv*, abs/2010.11929.

Bent Fuglede and Flemming Topsoe. 2004. Jensen-shannon divergence and hilbert space embedding. In *International symposium onInformation theory, 2004. ISIT 2004. Proceedings.*, page 31. IEEE.

Carolina Galleguillos, Andrew Rabinovich, and Serge Belongie. 2008. Object categorization using co-occurrence, location and appearance. In *2008 IEEE Conference on Computer Vision and Pattern Recognition*, pages 1–8. IEEE.

Tianrui Guan, Fuxiao Liu, Xiyang Wu, Ruiqi Xian, Zongxia Li, Xiaoyu Liu, Xijun Wang, Lichang Chen, Furong Huang, Yaser Yacoob, Dinesh Manocha, and Tianyi Zhou. 2023. Hallusionbench: An advanced diagnostic suite for entangled language hallucination and visual illusion in large vision-language models. *2024 IEEE/CVF Conference on Computer Vision and Pattern Recognition (CVPR)*, pages 14375–14385.

Kaiming He, Georgia Gkioxari, Piotr Dollár, and Ross Girshick. 2018. Mask r-cnn. *Preprint*, arXiv:1703.06870.

Qidong Huang, Xiao wen Dong, Pan Zhang, Bin Wang, Conghui He, Jiaqi Wang, Dahua Lin, Weiming Zhang, and Neng H. Yu. 2023. Opera: Alleviating hallucination in multi-modal large language models via over-trust penalty and retrospection-allocation. *2024 IEEE/CVF Conference on Computer Vision and Pattern Recognition (CVPR)*, pages 13418–13427.

Drew A. Hudson and Christopher D. Manning. 2019. Gqa: a new dataset for compositional question answering over real-world images. *ArXiv*, abs/1902.09506.

Fushuo Huo, Wenchao Xu, Zhong Zhang, Haozhao Wang, Zhicheng Chen, and Peilin Zhao. 2025. Self-introspective decoding: Alleviating hallucinations for large vision-language models. *Preprint*, arXiv:2408.02032.

Zhehan Kan, Ce Zhang, Zihan Liao, Yapeng Tian, Wenming Yang, Junyuan Xiao, Xu Li, Don San Jiang, Yaowei Wang, and Qingmin Liao. 2024. Catch: Complementary adaptive token-level contrastive decoding to mitigate hallucinations in lmlms. *ArXiv*, abs/2411.12713.

Alexander Kirillov, Eric Mintun, Nikhila Ravi, Hanzi Mao, Chloé Rolland, Laura Gustafson, Tete Xiao, Spencer Whitehead, Alexander C. Berg, Wan-Yen Lo, Piotr Dollár, and Ross B. Girshick. 2023. Segment anything. *2023 IEEE/CVF International Conference on Computer Vision (ICCV)*, pages 3992–4003.

Ranjay Krishna, Yuke Zhu, Oliver Groth, Justin Johnson, Kenji Hata, Joshua Kravitz, Stephanie Chen, Yannis Kalantidis, Li-Jia Li, David A. Shamma, Michael S. Bernstein, and Li Fei-Fei. 2016. Visual genome: Connecting language and vision using crowdsourced dense image annotations. *International Journal of Computer Vision*, 123:32 – 73.

Sicong Leng, Hang Zhang, Guanzheng Chen, Xin Li, Shijian Lu, Chunyan Miao, and Li Bing. 2023. Mitigating object hallucinations in large vision-language models through visual contrastive decoding. *2024 IEEE/CVF Conference on Computer Vision and Pattern Recognition (CVPR)*, pages 13872–13882.

Bo Li, Kaichen Zhang, Hao Zhang, Dong Guo, Renrui Zhang, Feng Li, Yuanhan Zhang, Ziwei Liu, and Chunyuan Li. 2024. Llava-next: Stronger llms supercharge multimodal capabilities in the wild.

Xiang Lisa Li, Ari Holtzman, Daniel Fried, Percy Liang, Jason Eisner, Tatsunori Hashimoto, Luke Zettlemoyer, and Mike Lewis. 2022. Contrastive decoding: Open-ended text generation as optimization. In *Annual Meeting of the Association for Computational Linguistics*.

Yifan Li, Yifan Du, Kun Zhou, Jinpeng Wang, Wayne Xin Zhao, and Ji rong Wen. 2023. Evaluating object hallucination in large vision-language models. In *Conference on Empirical Methods in Natural Language Processing*.

Tsung-Yi Lin, Michael Maire, Serge J. Belongie, James Hays, Pietro Perona, Deva Ramanan, Piotr Dollár, and C. Lawrence Zitnick. 2014. [Microsoft coco: Common objects in context](#). In *European Conference on Computer Vision*.

Hanchao Liu, Wenyuan Xue, Yifei Chen, Dapeng Chen, Xiutian Zhao, Ke Wang, Liping Hou, Rong-Zhi Li, and Wei Peng. 2024a. [A survey on hallucination in large vision-language models](#). *ArXiv*, abs/2402.00253.

Haotian Liu, Chunyuan Li, Yuheng Li, and Yong Jae Lee. 2023. [Improved baselines with visual instruction tuning](#). In *2024 IEEE/CVF Conference on Computer Vision and Pattern Recognition (CVPR)*, pages 26286–26296.

Shiping Liu, Kecheng Zheng, and Wei Chen. 2024b. [Paying more attention to image: A training-free method for alleviating hallucination in l4lms](#). *ArXiv*, abs/2407.21771.

Yang Liu, Peng Sun, Nickolas Wergeles, and Yi Shang. 2021. A survey and performance evaluation of deep learning methods for small object detection. *Expert Systems with Applications*, 172:114602.

Anna Rohrbach, Lisa Anne Hendricks, Kaylee Burns, Trevor Darrell, and Kate Saenko. 2018. [Object hallucination in image captioning](#). In *Conference on Empirical Methods in Natural Language Processing*.

Dustin Schwenk, Apoorv Khandelwal, Christopher Clark, Kenneth Marino, and Roozbeh Mottaghi. 2022. [A-okvqa: A benchmark for visual question answering using world knowledge](#). In *European Conference on Computer Vision*.

Xintong Wang, Jingheng Pan, Liang Ding, and Christian Biemann. 2024. [Mitigating hallucinations in large vision-language models with instruction contrastive decoding](#). *ArXiv*, abs/2403.18715.

Sangmin Woo, Jaehyuk Jang, Donguk Kim, Yubin Choi, and Changick Kim. 2024. [Ritual: Random image transformations as a universal anti-hallucination lever in large vision language models](#).

Shukang Yin, Chaoyou Fu, Sirui Zhao, Ke Li, Xing Sun, Tong Xu, and Enhong Chen. 2023. [A survey on multimodal large language models](#). *National Science Review*, 11.

Qifan Yu, Juncheng Li, Longhui Wei, Liang Pang, Wentao Ye, Bosheng Qin, Siliang Tang, Qi Tian, and Yueting Zhuang. 2023. [Hallucidocor: Mitigating hallucinatory toxicity in visual instruction data](#). In *2024 IEEE/CVF Conference on Computer Vision and Pattern Recognition (CVPR)*, pages 12944–12953.

Zihao Yue, Liang Zhang, and Qin Jin. 2024. [Less is more: Mitigating multimodal hallucination from an EOS decision perspective](#). In *Proceedings of the 62nd Annual Meeting of the Association for Computational Linguistics (Volume 1: Long Papers)*, pages 11766–11781, Bangkok, Thailand. Association for Computational Linguistics.

Jiarui Zhang, Jinyi Hu, Mahyar Khayatkhoei, Filip Ilievski, and Maosong Sun. 2024. [Exploring perceptual limitation of multimodal large language models](#). *ArXiv*, abs/2402.07384.

Zhiyuan Zhao, Bin Wang, Linke Ouyang, Xiao wen Dong, Jiaqi Wang, and Conghui He. 2023. [Beyond hallucinations: Enhancing l4lms through hallucination-aware direct preference optimization](#). *ArXiv*, abs/2311.16839.

Yiyang Zhou, Chenhang Cui, Jaehong Yoon, Linjun Zhang, Zhun Deng, Chelsea Finn, Mohit Bansal, and Huaxiu Yao. 2024. [Analyzing and mitigating object hallucination in large vision-language models](#). *Preprint*, arXiv:2310.00754.

A Implementation Details

POPE Setting

For the POPE evaluation, 500 images are randomly selected from each of MS-COCO, AOKVQA and GQA. Each dataset is divided into three subsets based on different questioning strategies: Random, Popular, and Adversarial. In each subset, each image is paired with six distinct queries, resulting in a total of 3000 queries. The three datasets together contain a total of 27,000 queries. The hyperparameter α is set in the range of 0.1 to 0.6 for LLaVA-1.5 and InstructBLIP, while for LLaVA-NeXT, it is adjusted within the range of 1.0 to 1.6. The N in Equation 5 is set to $0.05 * n$ in Equation 4. Beam Search is employed with a beam size of 2, and the temperature is set to 1 under multinomial decoding. OPERA, being designed based on beam search, does not produce results under greedy decoding and multinomial decoding settings.

CHAIR Setting

For the CHAIR evaluation, we randomly select 500 images from the MS-COCO dataset and generate image captions using our method as well as other decoding methods for evaluation. For fairness, VCD, OPERA, HALC and our HDD are all evaluated under the beam search setting with respective default settings, and their performance is compared with the original model using different decoding strategies, including greedy decoding, beam search, and multinomial sampling. The α is set within the range of 0.1 to 0.6, the N in Equation 5 is set to $0.05 * n$ in Equation 4, the *max new tokens* is set to 64 across all methods and the temperature is set to 1 under multinomial decoding.

GPT-4 Assisted Benchmark Setting

We randomly selected 200 images from the VG dataset and used the prompt ‘*Please describe the image in detail.*’ to obtain the model’s description of the images. The descriptions were then evaluated by GPT-4 for fine-grained assessment. Our GPT-4 Assisted Benchmark is based on HalluBench (Zhao et al., 2023). The detailed prompt settings will be presented in Table 5. For fairness, VCD, OPERA, and our HDD are all evaluated under the beam search setting. The α is set within the range of 0.1 to 0.6, the N in Equation 5 is set to $0.05 * n$ in Equation 4, the *max new tokens* is set to 512 across all methods and the temperature is set to 1 under multinomial decoding.

B Adaptive Plausibility Constraints

In Equation 2, the segmented images v_i perform visual enhancement on the original image, but these segmented images are not always reasonable in every situation. This uncertainty amplifies the uncertainty in the model’s output distribution, ultimately leading to implausible outputs. To address this issue, We implemented an adaptive consistency constraint following (Li et al., 2022), which depends on the confidence level associated with the output distribution relative to the original visual input. The mathematical form is as follows:

$$C_{head}(y_{<t}) = \{y_t \in \mathcal{C} : p(y_t|v, x, y_{<t}) \geq \beta \max_w p(w|v, x, y_{<t})\} \quad (11)$$

where β is a hyperparameter in the range of [0,1], we set β to 0.1 across all experiments.

C Ablation Studies

C.1 Distribution of δ

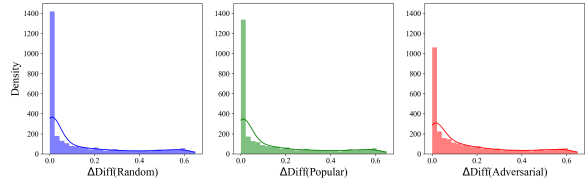


Figure 7: This figure illustrates the distribution of δ for LLaVA-1.5 on MS-COCO. The three subplots represent the distribution of δ across the Random, Popular, and Adversarial subsets.

The values of δ are mainly distributed within the range of 0 to 0.6, with nearly half of the δ values concentrated near 0 (each subset contains 3000 queries). This occurs because, in the POPE evaluation, half of the queries have the answer ‘No’. When such queries, along with two segmented images, are input into LVLMs, both segmented images should have a logit distribution similar to that of a blank image (since neither image contains the object mentioned in the query), resulting in a δ close to 0. Compared to the Random subset, the Popular and Adversarial subsets show fewer values near 0, as the entities queried in the Popular and Adversarial subsets are more likely to induce hallucinations in the LVLM. This Figure 7 essentially represents the distribution of positive and negative samples in the dataset.

C.2 Effect of Parameter α

Table 4 presents the POPE evaluation results with different alpha values in Equation 9 (showing re-

α	ACC \uparrow	F1 \uparrow	Yes Ratio(%)
0.2	88.1 $(+4.8)$	87.4 $(+6.1)$	44.6
0.4	88.9 $(+5.6)$	88.6 $(+7.3)$	47.1
0.6	89.3 $(+6.0)$	89.2 $(+7.9)$	49.2
0.8	89.1 $(+5.8)$	89.2 $(+7.9)$	50.4
1.0	88.9 $(+5.6)$	89.0 $(+7.7)$	51.7
vanilla	83.3	81.3	39.7

Table 4: Ablation study of α on the POPE benchmark

sults for LLaVA-1.5 on the MS-COCO random subset, using multinomial sampling with a temperature setting of 1). We selected a range from 0.2 to 1.0 with a step size of 0.2. The impact of different alpha settings on the results is minimal, with stable results across the range of alpha from 0.2 to 1.0, all significantly outperforming the baseline setting. This demonstrates that our method exhibits good consistency and stability across different alpha settings.

C.3 CHAIR Recall Analysis

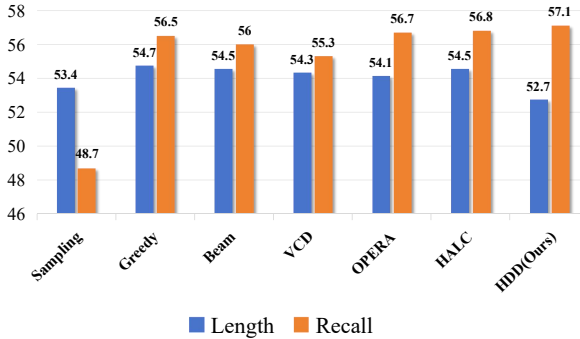


Figure 8: This chart illustrates the Recall and Length metrics of various decoding methods in the CHAIR evaluation for LLaVA-1.5.

Building on CHAIR, we followed the design of (Yue et al., 2024) to compute the Recall values for each setting, in order to assess the semantic richness of the model’s generated statements. As shown in the results in Figure 8, With a similar generation length, HDD achieved the highest recall value, surpassing the default decoding settings by 17.2%. Combining the CHAIR evaluation results in Table 2, our HDD generates more effective information and fewer hallucinations per unit length of description.

D More Case Studies

More case studies are shown in Figure 9.

GPT-4 Assisted Benchmark Prompt

Please help me judge if the comment of this image is hallucination or correct. I will give you a list of region description of a image. The format is [x1, y1, x2, y2]: region description, where [x1, y1, x2, y2] is the bounding box of the region. Highly overlapping bounding boxes may refer to the same object. This is the ground truth information of the image. Besides, I give you some factual information about the content of the image (which is 100% accurate). Your judgement should base on this information. However, this information only describe the objects in the region of image, so it cannot describe the subjective part of the image, e.g., atmosphere, style, emotion. In that case, you can return "Cannot judge".

Also, I will give you a list of comments of the image for you to judge if it is hallucination. Please give a judgement one by one along with the reason.

Your output should be:

Judgement:

1. hallucination or correct or cannot judge: <reason>
2. ...

Here are the region descriptions of the image:

{}

Factual Information:

{}

Here is the comment for you to judge (hallucination, correct, or cannot judge):

{}

Table 5: The prompt used for GPT-4 Assisted Benchmark



Vanilla:

The image features a woman standing in a room, holding a red suitcase in her hand. She is wearing a dress and appears to be preparing for a trip or a journey. The room has a chair positioned nearby, and a handbag can be seen placed on the floor. The woman's outfit and the presence of the luggage suggest that she is ready to leave for her destination.

Ours:

The image features a woman standing in a room, holding a red suitcase in her hand. She is positioned near a chair, which is located on the left side of the room. The suitcase is placed close to her, and she appears to be either preparing to leave or has just arrived. The woman's outfit includes a dress, which complements the overall scene.



Vanilla:

The image features a group of people gathered around a green bus, which is parked on the side of a road. The bus appears to be filled with various items, possibly for a trip or an event. There are several people standing around the bus, with some of them holding umbrellas, possibly to protect themselves from the sun or rain. In addition to the bus, there are multiple bicycles scattered around the scene, with some parked close to the bus and others further away. A few backpacks can also be seen, likely belonging to the people gathered around the bus. A car is parked in the background, and a person is sitting on the ground, possibly resting or observing the scene. The overall atmosphere suggests a lively gathering or event involving the bus and its contents.

Ours:

The image depicts a group of people gathered around a green bus, which is parked on the side of a road. The bus is loaded with various items, including bicycles and backpacks. There are several bicycles scattered around the bus, with some placed close to the bus and others further away. There are numerous people standing around the bus, some of them closer to the bus while others are further away. A few people are standing near the back of the bus, while others are closer to the front. Some people are also sitting on the grass, possibly taking a break or waiting for the bus to continue its journey. In the background, there is a car parked further down the road, and a stop sign can be seen near the left edge of the image.



Vanilla:

The image features a woman sitting on a wooden bench in a park, surrounded by greenery. She is reading a book, enjoying her time in the serene environment. The bench is positioned near a fountain, adding to the peaceful atmosphere. There are several potted plants in the scene, with one located close to the bench and others scattered throughout the park. The woman appears to be the main focus of the image, as she is the only person visible in the scene.

Ours:

The image features a woman sitting on a wooden bench in a park, enjoying the view of a fountain. She is reading a book while relaxing on the bench. The bench is located near the center of the scene, and the woman is positioned towards the right side of the bench. The park is adorned with greenery, including a few bushes and trees surrounding the area. The fountain is located on the left side of the scene, adding a soothing ambiance to the park.



Vanilla:

The image features a dining table with a white plate containing a delicious sandwich and a salad. The sandwich is cut in half, revealing its contents, and is accompanied by a side of salad. The salad is served in a bowl, and there are several pieces of broccoli scattered around the plate. The table is set with various utensils, including a fork, a knife, and a spoon. There are also two cups on the table, one near the top left corner and the other near the top right corner. A chair is positioned in front of the table, ready for someone to sit and enjoy the meal.

Ours:

The image features a dining table with a white plate containing a delicious sandwich and a salad. The sandwich is cut in half, revealing its contents, and is accompanied by a side of salad. The salad is served in a bowl, and there are several garnishes, including olives, scattered around the plate. In addition to the main dish, there are a few cups on the table, one of which is filled with water. A knife and a fork are also present on the table, ready for use. The dining table is surrounded by several chairs, indicating that it is set for a meal with friends or family.

Figure 9: This figure presents more examples of LLaVA-1.5 on MS-COCO, with hallucinated information highlighted in Red.